HHS Public Access

Author manuscript

Mamm Genome. Author manuscript; available in PMC 2020 June 01.

Published in final edited form as:

Mamm Genome. 2019 June ; 30(5-6): 151–165. doi:10.1007/s00335-019-09802-7.

Chronic and age-dependent effects of the spongiform neurodegeneration-associated MGRN1 E3 ubiquitin ligase on mitochondrial homeostasis

Teresa M. Gunn, **Derek Silvius**, **Andrew Lester**, and **Britney Gibbs**

McLaughlin Research Institute, Great Falls, MT USA

Abstract

Spongiform encephalopathy is an intriguing yet poorly understood neuropathology characterized by vacuoles, demyelination, and gliosis. It is observed in patients with prion disease, primary mitochondrial disease, HIV-1 infection of the brain, and some inherited disorders, but the underlying mechanism of disease remains unclear. The brains of mice lacking the MGRN1 E3 ubiquitin ligase develop vacuoles by 9 months of age. MGRN1-dependent ubiquitination has been reported to regulate mitofusin 1 and GP78, suggesting MGRN1 may have a direct effect on mitochondrial homeostasis. Here, we demonstrate that some MGRN1 localizes to mitochondria, most likely due to N-myristoylation, and mitochondria in cells from *Mgrn1* null mutant mice display fragmentation and depolarization without recruitment of the parkin E3 ubiquitin ligase. The late onset of pathology in the brains of *Mgrn1* null mutant mice suggests that a further, age-dependent effect on mitochondrial homeostasis may be required to trigger vacuolation. Parkin protein and mRNA levels showed a significant decline in the brains of *Mgrn1* null mutant mice by 12 months of age. To test whether loss of parkin triggers vacuolation through a synergistic effect, we generated *Mgrn1; parkin* double mutant mice. By 1 month of age, their brains demonstrated more severe mitochondrial dysfunction than *Mgrn1* null mutants, but there was no effect on the age-of-onset of spongiform neurodegeneration. Expression of the ATF4 transcription factor, a key regulator of the mitochondrial stress response, also declined in the brains of aged *Mgrn1* null mutant mice. Together, the data presented here indicate that loss of MGRN1 has early, direct effects on mitochondrial homeostasis and late, indirect effects on the ability of cells to respond to mitochondrial stress.

Introduction

Oxidative phosphorylation in mitochondria provides cells with most of their energy in the form of adenosine triphosphate (ATP). As the mammalian brain consumes especially high amounts of energy to drive neuronal activity, it is not surprising that the CNS is the second

Correspondence to: Teresa Gunn, tmg@mclaughlinresearch.org, McLaughlin Research Institute, 1520 23rd St S., Great Falls, MT 59404 USA, Tel: 406-454-6033, Fax: 406-454-6019.

Conflict of Interest Statement

On behalf of all authors, the corresponding author states that there is no conflict of interest.

most frequently affected organ in patients with mitochondrial disease (Finsterer, 2006). Mitochondria are dynamic organelles: they exist in networks that undergo continual remodeling through fusion and fission, migrate throughout the cell, and undergo regulated turnover (Chen and Chan, 2009; Meyer et al., 2017). Disruption of mitochondrial dynamics leads to mitochondrial dysfunction and predominantly affects tissues with high energy requirements (i.e., heart, brain, skeletal muscle, liver and kidney). Mitophagy regulates mitochondrial homeostasis by eliminating damaged, aged or surplus mitochondria (Ashrafi and Schwarz, 2013; Chen and Chan, 2009). Two genes associated with familial Parkinson's disease, PINK1 and parkin, regulate mitochondrial dynamics and the clearance of damaged mitochondria through mitophagy (Dagda et al., 2009; Deng et al., 2008; Exner et al., 2007; Gautier et al., 2008; Narendra et al., 2008; Poole et al., 2008), but parkin-independent mitophagy pathways also play critical roles in maintaining mitochondrial homeostasis (Villa et al., 2018).

Patients with Leigh syndrome, a genetically heterogeneous mitochondrial disorder, show progressive neurological deterioration characterized histologically by multifocal spongiform degeneration, demyelination, and gliosis (Ruhoy and Saneto, 2014). Mice lacking the mahogunin ring finger-1 (MGRN1) E3 ubiquitin ligase develop late-onset, progressive CNS vacuolation with gliosis (He et al., 2003) histopathologically similar to that caused by primary mitochondrial disease. Vacuoles first appear in the CNS of mice homozygous for a null allele, *Mgrn1*$^{md\text{-}nc}$, by 9 months of age and become larger and more numerous with age. Mitochondrial dysfunction (reduced cytochrome c oxidase activity and ATP levels), is apparent in the brains of *Mgrn1*$^{md\text{-}nc/md\text{-}nc}$ mice by 1 month-of-age (Sun et al., 2007), but it is unclear whether this is the primary cause of CNS vacuolation (Jiao et al., 2009a; Walker et al., 2016).

MGRN1 has been reported to affect mitophagy though ubiquitin-mediated regulation of GP78 levels (Mukherjee and Chakrabarti, 2016b), and to mediate mitofusin-1-dependent mitochondrial fusion (Mukherjee and Chakrabarti, 2016a). Age-dependent effects of MGRN1 on the expression of stress response genes has also been described (Benvegnu et al., 2017). These studies suggest MGRN1 may play a primary role in maintaining mitochondrial homeostasis. We examined whether loss of MGRN1 function alters mitochondrial morphology or membrane potential. Mitochondrial fragmentation and reduced tetramethylrhodamine, ethyl ester (TMRE) staining without parkin recruitment was observed in cells from *Mgrn1* null mutant mice and in cells over-expressing catalytically inactive (dominant negative) MGRN1. We discovered that parkin expression declined to undetectable levels in the brains of *Mgrn1* null mutant mice by 12 months of age, suggesting that loss of parkin-dependent mitophagy might exacerbate mitochondrial dysfunction to trigger the onset of CNS vacuolation. To test this hypothesis, we generated *Mgrn1* null mutant mice with congenital *parkin* deletion and examined their brains for spongiform neurodegeneration. Although no effect was seen on age-of-onset, thalamic vacuolation progressed more rapidly in the brains of *Mgrn1* null mutant mice lacking parkin. Our results indicate that loss of MGRN1 has chronic and age-dependent effects on mitochondrial homeostasis, and support a role for mitochondrial dysfunction in the pathogenesis of spongiform neurodegeneration, most likely by impacting cellular pathways that require high levels of ATP.

Methods

Mice

Mgrn1$^{md\text{-}nc/md\text{-}nc}$ (null) mutant mice (RRID:MGI:3704004) and co-isogenic controls have been described previously (He et al., 2003; Silvius et al., 2013). Our in-house colony has been maintained by brother-sister inbreeding of *Mgrn1*$^{md\text{-}nc}$ heterozygotes to homozygotes for over 60 generations. Animals were genotyped for the *Mgrn1*$^{md\text{-}nc}$ mutation using allele-specific PCR as follows: wildtype primers: GCCTGCATGGATAGATGGAT and AGGAAGTTGCCCACAAGAACGCA; mutant primers: CAAGAACAACCAGGAGACTAAGGA and GCCCAAGTCCTAAACCTCT; amplification using Promega GoTaq green 2X master mix and 10 cycles with an annealing temperature of 60 C followed by 30 cycles with an annealing temperature of 57 C. *Parkin (park2)* null mutant mice (B6.129S4-*Park2*^{tm1Shn}/J, RRID:IMSR_JAX:006582) were obtained from the Jackson Laboratory and genotyped according to the standard PCR protocol (https://www.jax.org/strain/006582). All animal procedures adhered to the US National Research Council's Guide for the Care and Use of Laboratory Animals, the US Public Health Service's Policy on Humane Care and Use of Laboratory Animals, the Guide for the Care and Use of Laboratory Animals, and were approved by the McLaughlin Research Institute Institutional Animal Care and Use Committee (IACUC).

Histology

Brains were fixed in 10% formalin for at least 1 week prior to standard processing and embedding in paraffin. Care was taken to not incubate specimens in 70% ethanol for more than 1 h and to process mutant and control samples together as prolonged exposure to 70% ethanol can cause artifactual vacuolation in rodent brain samples (Wells and Wells, 1989). Coronal sections were taken at 5 μm and stained with hematoxylin and eosin (H&E). For each brain region, 6 different sections from 2–4 different animals of each genotype were scored for vacuolation by counting the number of vacuoles in the field of view at 20X magnification on a Zeiss AxioImagerM1 microscope. Scoring was as follows: 0 = no significant lesions (0–1 vacuoles); 1 = rare, scattered vacuoles (2–5 vacuoles, not present in all fields of view); 2 = mild, 6–10 scattered vacuoles in all fields of view; 3 = moderate, vacuoles in every field of view and 11–29 evenly scattered vacuoles in most; 4 = severe, > 30 vacuoles in all fields of view.

Cell culture

Cell lines: HeLa (ATCC Cat# CRM-CCL-2, RRID:CVCL_0030), HEK293T (ATCC Cat# CRL-3216, RRID:CVCL_0063) and Neuro2a (ATCC Cat# CCL-131, RRID:CVCL_0470). Mouse embryonic fibroblasts (MEFs) were isolated from E12.5 *Mgrn1* null (*Mgrn1*$^{md\text{-}nc/md\text{-}nc}$) and coisogenic wildtype mouse embryos following standard protocols. MEFs, HeLa, HEK293T and Neuro2a cells were cultured under standard conditions (5% CO2 in DMEM with 10% fetal calf serum, penicillin and streptomycin). Immortalized *Mgrn1* null and wildtype melanocytes (melan-md1, melan-md2 and melan-a) were obtained from the Wellcome Trust Functional Genomics Cell Bank and have been described previously (Hida et al., 2009). They were cultured in RPMI containing 10% fetal calf serum and 200 nM tetradecanoyl phorbol acetate. HeLa cells and MEFs were transfected using

JetPrime transfection reagent (Polyplus Transfection, Inc.). HEK293T and Neuro2a cells were transfected following a standard calcium phosphate protocol. All experiments were performed at least 3 independent times to ensure consistent results. The wildtype and C278A/C281A (herein referred to as AVVA) mutant MGRN1-GFP constructs used in these studies were described previously (Jiao et al., 2009b), and the empty pEGFP-N1 vector (Clontech) was used as a control. Wildtype and G2A MGRN1-HIS constructs were a gift from Rudy Leibel and John Overton. YFP-parkin and mCherry-Parkin were gifts from Richard Youle (Addgene plasmids # 23955 and 23956). Mitochondria were visualized using MitoTracker red CMXRos or MitoTracker green FM (ThermoFisher Scientific) or immunofluorence for COXIV. For studies involving m-chlorophenylhydrozone (CCCP), cells were stained (preloaded) with MitoTracker red CMXRos and either left untreated or treated with 10 μM CCCP (Sigma-Aldrich) or dimethyl sulfoxide (DMSO, vehicle control; Sigma-Aldrich). Lysosomes (acidic organelles) were visualized using LysoTracker Red DND-99 (ThermoFisher Scientific).

Mitochondrial studies

To isolate mitochondria, brains or cell pellets were homogenized on ice in homogenization buffer (0.32 M sucrose, 1mM EDTA, 10mM Tris-HCL, pH 7.8), using a dounce-type glass homogenizer. The homogenate and subsequent supernatent were centrifuged at 1000 *g* for 10 min at 4 C to pellet nuclear material. The supernatent from the second spin was centrifuged for 20 minutes at 13000 *g*, at 4 C to obtain a crude mitochondrial pellet, which was resuspended in homogenization buffer and centrifuged for another 10 minutes at 13000 *g* at 4 C to obtain the mitochondrial pellet. For sodium bicarbonate treatment, each mitochondrial pellet was resuspended in 50 μl of ice-cold PBS with protease inhibitor (Roche), mixed with 500ul of carbonate buffer (fresh, cold 0.1M Na_2CO_3, pH 11), and incubated on ice for 15 minutes. Mitochondrial membranes were pelleted by centrifugation at 52,000 rpm for 10 minutes at 4 C and resuspended in 1X tris-glycine SDS sample buffer prior to SDS-PAGE. For proteinase K treatment, pellets were resuspended in homogenization buffer containing 1 mg/ml proteinase K (1mg/ml) and incubated at 37 C for 15 minutes. The reaction was stopped by adding 2 μl of 100mM phenylmethylsulfonyl floride. For trypsin treatment, mitochondrial pellets were resuspended in buffer (10 mM Hepes-KOH (pH 7.4), 250 mM sucrose, 0.5 mM, 2mM EGTA, and 1mM DTT) to a concentration of 1 mg/ml, then incubated with trypsin (10ug/ml) for 20 minutes at room temperature. Digestion was stopped by adding an equivalent amount of bovine trypsin inhibitor (Invitrogen). Proteinase K and trypsin samples were diluted 1:1 with 2X trisglycine SDS sample buffer prior to SDS-PAGE.

To quantify mitochondrial morphology in melanocytes and MEFs, mid-plane images of cells stained with MitoTracker green FM or MitoTracker red CMXRos were obtained using an Olympus Fluoview 2000 confocal microscope. Images were exported as tiff files and analyzed in ImageJ by manually setting the threshold to outline the majority of mitochondria within cells, then measuring area and perimeter using the “analyze particles” function. Tetramethylrhodamine, ethyl ester (TMRE; ThermoFisher Scientific) staining was performed on cells 1–3 days after transfection and cells imaged on an Olympus Fluoview 2000 confocal microscope.

Cytochrome c oxidase activity and ATP levels were determined in triplicate, as previously described (Sun et al., 2007). Briefly, mitochondria were isolated from freshly dissected brains and resuspended in ice-cold buffer (210mM mannitol, 70mM sucrose, 10mM HEPES, 1mM EDTA, 0.5mMdithiothreitol) without protease inhibitor. Protein concentration was determined by BCA protein assay (Pierce/ThermoFisher Scientific) and Complex IV activity determined on equal amounts of protein for each mitochondrial extract using the Cytochrome *c* Oxidase Assay kit (Millipore-Sigma). For ATP levels, brain hemispheres were homogenized in 10% perchloric acid, neutralized with 2.5M potassium hydroxide, and precipitates removed by centrifugation. Protein concentration of diluted supernatants was determined by BCA protein assay and ATP levels were assayed using the ATP Bioluminescent Assay kit (Millipore-Sigma) on equal amounts of brain proteins.

Immunoblotting

Brains and cells were homogenized in lysis buffer (50 mM Tris, 150 mM NaCl, 1% NP40, 0.1% sodium deoxycholate) supplemented with Complete protease inhibitor cocktail (Roche). Cellular debris was pelleted by centrifugation and the supernatant diluted in 2X SDS loading buffer. Mitochondrial fractions and supernatents were prepared as described above. Proteins were electrophoresed through SDS-polyacrylamide gels and transferred to Immobilon P membrane (Millipore). Western blotting (WB) was performed following standard protocols using the following antibodies: rabbit anti-MGRN1 (PTG labs #11285–1AP, RRID:AB_2143351), MitoProfile total OXPHOS rodent antibody cocktail (MitoSciences #MS604, RRID:AB_2629281), mouse anti-GFP (NeuroMab clone 86/8, RRID:AB_2313651), rabbit anti-MFN2 (Abcam ab124773, RRID:AB_10999860), mouse anti-parkin (PRK8) (Santa Cruz Biotechnology #sc-32282, RRID:AB_628104), and mouse anti-beta-tubulin (3F3-G2) (Santa Cruz Biotechnology #sc-53140, RRID:AB_793543).

Immunofluorescence

Cells were fixed in 4% paraformaldehyde for 10 min and permeabilized 10 min with 0.1% Triton X-100. Immunofluorescence (IF) was performed following standard protocols and the following antibodies: rabbit anti-MGRN1 from Proteintech Group, (cat. #11285–1-AP, RRID: AB_2143351), mouse anti-6*XHIS tag from Abcam (cat. #ab7857, RRID: AB_2716573), rabbit anti-COX IV (3E11) from Cell Signaling Technology (cat. #4850, RRID: AB_2085424), Alexa Fluor 488 conjugated goat anti-mouse IgG (Cell Signaling Technology cat. #4412, RRID:AB_1904025) and Alexa Fluor 647 conjugated goat anti-rabbit IgG (Cell Signaling Technology cat. #4414, RRID: AB_10693544).

Quantitative RT-PCR

Brains from 12 and 16 month-old *Mgrn1*$^{md\text{-}nc/md\text{-}nc}$ and *Mgrn1*$^{+/+}$ mice (3 of each genotype at each age) were homogenized in Trizol reagent (Invitrogen) and DNase-I treated RNA was isolated using the Direct-zol RNA miniprep kit (Zymo Research). Equal amounts of RNA were used as template for cDNA synthesis (Invitrogen SuperScript III First-Strand Synthesis kit), followed by amplification using SYBR green Brilliant II PCR master mix (Agilent) on a BioRad Opticon II. Expression of *Activating transcription factor 4 (Atf4)* and *parkin (Park2)* was normalized against *glucose phosphate isomerase (Gpi)* levels using the comparative $\Delta\Delta C_t$ method to determine the relative quantification value (Livak and

Schmittgen, 2001). All samples from mice at the same age were run in triplicate on the same plate. Primer sequences: Gpi-F CAACTGCTACGGCTGTGAGA, Gpi-R CTTTCCGTTGGACTCCATGT, parkin-F TGGAAAGCTCCGAGTTCAGT, parkin-R CCTTGTCTGAGGTTGGGTGT, Atf4-F GAAACCTCATGGGTTCTCCA, Atf4-R CATCCATTCGAAACAGAGCA.

Statistical analyses

Measures of mitochondrial morphology (area and perimeter), ATP levels, and cytochrome c oxidase activity were analyzed using Student's *t*-test. Differences in gene expression were analyzed using a one-tailed homoscedastic *t* test. Vacuolation scores were assessed by one-way ANOVA. For all studies, significance was set at $p < 0.05$.

Results

Mitochondrial defects associated with loss of MGRN1

Mitochondrial dysfunction (specifically, reduced ATP levels and cytochrome c oxidase activity) can be detected in the brains of *Mgrn1*$^{md\text{-}nc/md\text{-}nc}$ mice by 1 month of age (Sun et al., 2007). As MGRN1 has been reported to regulate mitofusin-1-dependent mitochondrial fusion (Mukherjee and Chakrabarti, 2016a), we assessed the effect of loss of MGRN1 on mitochondrial morphology in melanocytes and MEFs derived from wildtype or *Mgrn1* null mutant mice. Mitochondria were stained with MitoTracker green or MitoTracker red, imaged by confocal microscopy, and their morphology analyzed using ImageJ. In both cell types, the average mitochondrial area and perimeter was significantly lower in *Mgrn1* null cells compared to wildtype cells ($p \leq 0.005$; Fig. 1A–C), consistent with mitochondrial fragmentation.

Since mitochondrial fragmentation is typically associated with depolarization, we used tetramethylrhodamine, ethyl ester (TMRE) staining to determine whether absence of MGRN1 or overexpression of a dominant negative, catalytically inactive MGRN1 mutant (AVVA) was associated with reduced mitochondrial membrane potential. While MitoTracker green and TMRE staining overlapped almost completely in wildtype MEFs, colocalization was consistently reduced in *Mgrn1* null MEFs (Fig. 1D), indicating mitochondrial depolarization. In fact, the pattern of TMRE staining in untreated *Mgrn1* null MEFs was very similar to that of wildtype MEFs following treatment with the mitochondrial uncoupler, m-chlorophenylhydrozone (CCCP; data not shown). TMRE staining was also consistently reduced in HeLa cells over-expressing MGRN1^{AVVA}-GFP but not wildtype MGRN1-GFP (Fig. 1E), demonstrating a requirement for catalytically active MGRN1 in maintaining mitochondrial membrane potential.

Mitochondrial localization of MGRN1

MGRN1 is predicted to undergo N-myristoylation on a highly conserved glycine residue at amino acid position 2. N-myristoylation targets proteins to lipid membranes, and we had noticed, in multiple cell types, that some MGRN1 appeared to localize to mitochondria. To verify this, we stained HEK293T cells expressing MGRN1-GFP with MitoTracker Red or LysoTracker Red. All MitoTracker Red-stained structures appeared to be encircled by

MGRN1-GFP (Fig. 2A), whereas only a small subset of MGRN1-GFP colocalized with LysoTracker Red staining (Fig. 2B). Mitochondrial localization of MGRN1 in HeLa cells was also verified using GFP-tagged wildtype and catalytically inactive MGRN1-GFP with MitoTracker Red staining (Fig. 2C), as well as antibodies against endogenous MGRN1 and mitochondrial cytochrome c oxidase IV (COXIV), which localizes to the mitochondrial inner membrane (Fig. 2D). In all experiments, MGRN1 (wildtype and AVVA mutant) was distributed throughout the cytoplasm as well as on mitochondria, most likely on the outer membrane.

To test whether N-myristoylation of the glycine in position 2 of the amino acid sequence is responsible for targeting MGRN1 to mitochondria, HeLa cells were transfected with wildtype or myristoylation-defective (G2A mutant) MGRN1-HIS expression constructs. Immunofluorescence staining using antibodies against HIS or MGRN1 (to detect MGRN1-HIS) and COXIV (to visualize mitochondria) confirmed cytoplasmic and mitochondrial localization of wildtype MGRN1 (Fig. 3A), while G2A mutant MGRN1-HIS showed diffuse cytoplasmic expression that had little or no overlap with COXIV staining (Fig. 3B). Since MGRN1 does not have a mitochondrial import sequence, it is predicted to localize to the outer mitochondrial membrane. To verify this, mitochondria were isolated from untransfected HEK293T cells and cells transiently transfected to express GFP, MGRN1-GFP, or MGRN1^{AVVA}-GFP and treated with sodium bicarbonate. Proteins extracted from cell lysates (lane 1), mitochondrial fractions (lane 2), the sodium carbonate supernatent (peripheral mitochondrial proteins, lane 3), and the pellet (integral mitochondrial proteins, lane 4) were immunoblotted for MGRN1 (Fig. 3C). Endogenous and GFP-tagged MGRN1 were detected in the sodium bicarbonate pellet, with much lower levels detected in the supernatent fraction, suggesting mitochondrial MGRN1 is either very tightly associated with or integral to mitochondria. Catalytically inactive MGRN1 appeared to be more specifically and more tightly bound to mitochondria than wildtype MGRN1. Enzymatic digestion of mitochondrial fractions isolated from HEK293T cells indicated that MGRN1 is a tightly associated peripheral mitochondrial protein since some endogenous MGRN1 remained in the mitochondrial fraction after proteinase K treatment (lane 6), but not following trypsin treatment (lane 4) (Fig. 3D). In addition, overnight treatment of transfected HEK293T cells with CCCP led to complete loss of MGRN1-GFP and MGRN1^{AVVA}-GFP, as well as the outer mitochondrial membrane protein mitofusin-2 (MFN2) (Fig. 3E). GFP, which does not localize to mitochondria, was unaffected, and cells treated for 21 h with DMSO or the proteasomal inhibitor MG132 still expressed GFP, MGRN1-GFP, MGRN1^{AVVA}-GFP and MFN2 (Fig. 3E). These observations suggest that MGRN1-GFP and MGRN1^{AVVA}-GFP, like MFN2, remain associated with mitochondria in CCCP-treated cells and are degraded through mitophagy. It was surprising that no MGRN1-GFP or MGRN1^{AVVA}-GFP was detected after 21h of CCCP treatment since not all MGRN1-GFP or MGRN1^{AVVA}-GFP localized to mitochondria in untreated HEK293T cells (Fig. 2C). These results suggest that wildtype and catalytically inactive MGRN1 may be actively recruited to depolarized mitochondria. The fact that both MGRN1-GFP and MGRN1(AVVA)-GFP were lost from cells following 21h of CCCP treatment indicates that over-expression of the mutant isoform, which is predicted to act as a dominant negative, does not prevent mitophagy triggered by CCCP-induced depolarization.

To determine whether MGRN1-GFP could be used as a marker of mitochondria in studies using CCCP, transiently transfected HeLa cells expressing GFP, MGRN1-GFP or MGRN1^{AVVA}-GFP were pre-loaded with MitoTracker Red for 1 hour, then treated with 10 μM CCCP for 2–3 hours and imaged on the confocal microscope. In all CCCP treated cells, MitoTracker-stained mitochondria had a “rounded up” appearance that showed no colocation with GFP (empty vector), while wildtype and catalytically inactive MGRN1-GFP both remained localized to mitochondria (Fig. 4).

MGRN1-dependent mitochondrial dysfunction does not trigger parkin recruitment

Recruitment of parkin to pathologically depolarized mitochondria promotes their degradation through autophagy (Narendra et al., 2009). Since TMRE staining indicated that loss of MGRN1 or over-expression of catalytically inactive MGRN1 causes mitochondrial depolarization, we investigated whether this results in parkin recruitment. As neither MEFs nor melanocytes express endogenous parkin (Matsuda et al., 2010 and data not shown), *Mgrn1* null and wildtype MEFs and melanocytes were transfected with mCherry-parkin (mCh-parkin) or YFP-parkin and stained with MitoTracker green or MitoTracker Red. In untreated *Mgrn1* null and wildtype cells, parkin showed a diffuse cytoplasmic distribution (Fig. 5A–B, left panels). Following CCCP treatment, parkin colocalized with MitoTracker staining (Fig. 5A–B, right panels). Thus, while the disrupted mitochondrial membrane potential observed in *Mgrn1* null MEFs by TMRE staining does not trigger parkin-dependent mitophagy, CCCP treatment can still induce parkin recruitment in cells lacking MGRN1.

Using MGRN1-GFP to visualize mitochondria, we also examined parkin localization and recruitment to mitochondria in HeLa cells transiently transfected to overexpress wildtype or catalytically inactive MGRN1-GFP and mCh-parkin. Cells were imaged by confocal microscopy 1–2 days after transfection, then treated with 10 μM CCCP or DMSO and imaged again 2–3 hours later. No mitochondrial recruitment of mCh-parkin was observed prior to CCCP treatment or in DMS treated cells, even in cells over-expressing MGRN1^{AVVA}-GFP, whereas mCh-parkin colocalized with both wildtype and AVVA mutant MGRN1-GFP within 2 h of CCCP treatment, by which time the vast majority of mCh-parkin colocalized with MGRN1-GFP on mitochondria (Fig. 5C). The fact that parkin can localizes to depolarized mitochondria in the presence of catalytically inactive MGRN1 suggests its recruitment is not dependent on MGRN1-dependent ubiquitination.

Age-dependent effect of MGRN1 on parkin expression

Mitochondrial dysfunction is apparent in the brains of *Mgrn1* null mutant mice by 1 month of age, but they do not develop spongiform neurodegeneration until approximately 9 months of age. Since the CNS histopathology of *Mgrn1* null mutants is similar to that caused by primary mitochondrial disease, we hypothesized that a further, age-dependent decline in mitochondrial function in *Mgrn1* null brains may be required to trigger the onset of CNS vacuolation. Parkin levels have been reported to decline with age in the brains of rhesus monkeys (Yang et al., 2015), prompting us to examine parkin expression in the brains of wildtype and *Mgrn1* null mutant mice at a variety of ages (Fig. 6A). Parkin protein levels were similar in the brains of wildtype and *Mgrn1* null mice up to 9 months of age. By 12

months of age, parkin levels appeared to be slightly reduced in wildtype brains but were undetectable in *Mgrn1* mutant brains. Parkin mRNA levels were also significantly reduced, to approximately 50% (p=0.015) and 20% (p=0.002) of wildtype in the brains of 12 and 16 month old *Mgrn1* null mutant mice, respectively (Fig. 6B and Table 1).

A reduction in MGRN1 levels in hippocampal neurons between 5 and 24 months of age was recently reported, along with subcellular redistribution of MGRN1 from the cytoplasm to the nucleus (Benvegnu et al., 2017). The transcriptional consequences of increased nuclear MGRN1 were assessed by RNA sequencing analysis in HEK293T cells, which revealed preferential upregulation of genes involved in the cellular response to proteasomal stress, including activating transcription factor-3 (ATF3). ATF3 expression is activated by ATF4, which also regulates parkin expression. We therefore performed qRT-PCR to examine *Atf4* expression levels. At 12 months, there was a trend toward reduced *Atf4* expression in *Mgrn1* null brains relative to wildtype (approximately 60% of wildtype, p=0.211), while a significant decrease in expression was readily detected at 16 months of age (approximately 20% of wildtype, p=0.037) (Fig. 6B and Table 1).

Synergistic effects of parkin and MGRN1

The brains of *Mgrn1* and *parkin* null mutant mice have previously been shown to have significant reductions in several subunits of complex I of the mitochondrial electron transport chain, elevated levels of oxidative damage (protein carbonyls), and altered respiratory capacity or ATP levels (Palacino et al., 2004; Sun et al., 2007). The data presented here suggest that MGRN1 and parkin act through independent pathways to regulate mitochondrial homeostasis since disruption of MGRN1 does not trigger parkin-mediated mitophagy. Furthermore, we have shown that parkin levels decrease in the brains of *Mgrn1* null mice at about the same age at which CNS vacuoles appear. This suggested that loss of parkin-dependent regulation of mitochondrial homeostasis in the absence of MGRN1 may be sufficient to trigger the onset of spongiform neurodegeneration. To test this, we generated *Mgrn1; parkin* double mutants and examined whether they exhibit more severe mitochondrial dysfunction than either of the single mutants, and whether CNS vacuolation appears earlier than in the brains of mice lacking only MGRN1.

ATP levels and cytochrome c oxidase activity were assayed in the brains of 1 month-old wildtype, *Mgrn1* null, *parkin* null, and *Mgrn1; parkin* double mutant animals. *Mgrn1* null and double mutant brains had significantly reduced ATP levels (Fig. 7A). The difference in ATP levels between *Mgrn1* null mutants and double mutants was suggestive but not statistically significant (p=0.087). Cytochrome c oxidase activity was only significantly reduced in the brains of double mutant mice (Fig. 7B). These data are consistent with absence of MGRN1 and parkin causing more severe mitochondrial dysfunction than loss of either protein alone.

To test whether loss of parkin affects the onset of spongiform neurodegeneration, H&E stained coronal sections of brains from 6, 9 and 12 month-old *Mgrn1* null mutant mice homozygous for either the wildtype or null allele at the *parkin* (*park2*) locus were examined and scored for vacuoles as described in the Methods. No vacuolation was observed in the brains of 6 month-old mice of any genotype (data not shown). Mild vacuolation was

observed in the brains of all *Mgrn1* null mutants at 9 month-old of age, with no significant effect of *parkin* genotype on severity in any of the brain regions scored (Fig. 7C–D and Table 2). At 12 months of age, vacuolation was comparable in all brain regions except for the thalamus, where double mutants had significantly more vacuoles (average of 41 vacuoles per field of view vs. 19 in *Mgrn1* null mutants; p=0.017) (Fig. 7E–F and Table 2). No vacuoles were apparent in the brains of 12 month-old compound heterozygotes or *parkin* null mutant mice carrying at least 1 wildtype *Mgrn1* allele (data not shown). These results indicate that absence of parkin accelerates the progression of vacuolation in the thalamus of *Mgrn1* null mice but it does not affect the age at which vacuoles first appear, despite causing a more severe reduction in CNS ATP levels and cytochrome c oxidase activity by 1 month of age. It is not obvious why the effect of parkin is limited to the thalamus.

Discussion

The various phenotypes observed in mice lacking MGRN1 are not surprising given this protein's role in diverse cellular pathways. MGRN1 was recently identified as a negative regulator of sonic hedgehog signaling on primary cilia (Pusapati et al., 2018), which likely underlies the aberrant left-right patterning, congenital heart defects and abnormal cranioskeletal patterning observed in *Mgrn1* null mutant mice (Cota et al., 2006; Jiao et al., 2009a). MGRN1 has also been shown to regulate the endosomal sorting complex required for transport-I (ESCRT-I) protein, tumor susceptibility gene 101 TSG101 (Jiao et al., 2009b; Kim et al., 2007), and we recently demonstrated that deleting TSG101 from oligodendroglia causes rapid onset spongiform neurodegeneration (Walker et al., 2016). The later age-of-onset of vacuolation in *Mgrn1* null mice may reflect the fact that loss of MGRN1 only partially impairs TSG101 function and suggests that other, age-dependent events may be involved.

CNS vacuolation caused by loss of MGRN1 is similar to that observed in human patients with mitochondrial encephalopathies, mice lacking NADH dehydrogenase (ubiquinone) Fe-S protein 4 (*Ndufs4*), and mice expressing an N-terminal truncated fragment of peroxisome proliferative activated receptor, gamma, coactivator 1 alpha (*Ppargc1a*, also known as PGC-1α) in the absence of the full-length protein (Betts et al., 2004; Brown and Squier, 1996; Filosto et al., 2007; Leone et al., 2005; Quintana et al., 2010; Szalardy et al., 2013; Tanji et al., 2001). MGRN1 has been implicated in several pathways that regulate mitochondrial homeostasis and we have shown that *Mgrn1* null mutant mice have reduced brain ATP levels and their cells display mitochondrial fragmentation and depolarization. Since many steps in the ESCRT pathway are ubiquitin-dependent and ubiquitination requires ATP, chronic mitochondrial dysfunction caused by absence of MGRN1 could influence the onset of CNS vacuolation by further impairing ESCRT function. Alternatively, the comparatively late onset of spongiform neurodegeneration in *Mgrn1* mutant mice might reflect age-dependent changes in gene expression. In wildtype mice, overall MGRN1 levels declined with age and its cellular distribution shifted from the cytoplasm to the nucleus (Benvegnu et al., 2017). Proteasomal inhibition caused a similar relocalization of MGRN1 in neurons, and expression of MGRN1 in HEK293 cells following proteasomal inhibition led to up-regulation of several genes involved in the cellular response to proteasomal stress, including the *Atf3* transcription factor. *Atf4* expression is normally activated by

mitochondrial stress, and it in turn activates cytoprotective genes, including *parkin* and *Atf3* (Pan et al., 2003; Pan et al., 2007; Quiros et al., 2017). We detected a reduction in *Atf4* expression as well as that of one of its targets, *parkin,* in the brains of aged *Mgrn1* null mutant mice. Thus, absence of MGRN1 disrupts mitochondrial homeostasis, and aged *Mgrn1* null mutant mice are likely to be deficient in their ability to activate appropriate stress response pathways. Although congenital deletion of parkin did not alter the age of onset of CNS vacuolation in most brain regions in *Mgrn1* null mutant mice, *parkin* null mutant mice only demonstrate a mild mitochondrial defect that does not worsen with age (Damiano et al., 2014) and at least some aspects of mitochondrial homeostasis in mouse brain appear to be parkin-independent (Sterky et al., 2011). Altered expression of other ATF4 targets involved in stress response may play a role in the pathogenesis of spongiform neurodegeneration, but further studies will be required to address this.

A recent study reported a requirement for MGRN1-dependent ubiquitination of MFN1 on the outer mitochondrial membrane for normal mitochondrial fusion (Mukherjee and Chakrabarti, 2016a). The presence of mitochondrial fragmentation in cells lacking MGRN1 or over-expressing catalytically inactive MGRN1 is consistent with an effect of MGRN1 on MFN1 function. Although MEFs from *Mgrn1* null mice and HeLa cells over-expressing catalytically inactive MGRN1 showed mitochondrial depolarization, based on reduced TMRE staining, this was not associated with parkin recruitment. *Mfn1*$^{-/-}$ MEFs also display extensive mitochondrial fragmentation but no significant recruitment of parkin (Chen et al., 2005; Narendra et al., 2008). Parkin did translocate to depolarized mitochondria following CCCP treatment of cells lacking MGRN1 or expressing a catalytically inactive mutant, however, indicating that functional MGRN1 is not required for parkin recruitment. Further studies will be needed to determine whether mitochondrial dysfunction associated with loss of MGRN1 function triggers other, parkin-independent mitophagy pathways. Given that the brains of *Mgrn1* null mutant mice show an overall reduction in the levels of ATP and ubiquitinated proteins (Sun et al., 2007) and most mitophagy pathways in mammals are ubiquitin-dependent, MGRN1 could have an indirect effect on the ability of cells to clear damaged mitochondria.

Spongiform encephalopathy is an intriguing yet poorly understood neuropathology. It is most notably associated with prion disease, but also observed in patients with mitochondrial disorders and infection of the brain by some viruses, including human immunodeficiency virus (HIV-1). Mitochondrial dysfunction is a shared feature of each these diseases (Choi et al., 1998; Shah and Kumar, 2016; Siskova et al., 2010), suggesting it may play a causative role, but the cellular pathway(s) through which it acts remain to be identified. The fact that the brains of *Mgrn1* null mutant mice exhibit reduced ATP levels by one month of age but do not develop vacuoles until they are a year old suggests that mitochondrial dysfunction may need to reach a threshold of severity to trigger CNS vacuolation, or that other, mitochondrial-independent mechanisms such as prolonged disruption of TSG101 function, play an important role. The sensitized background of *Mgrn1* mutant mice will make them a useful model for identifying factors that influence the onset and progression of spongiform neurodegeneration and the downstream cellular mechanism(s) involved.

Acknowledgements

We are grateful to John Overton and Rudy Leibel for sharing MGRN1-HIS expression constructs, Anita Pecukonis and other McLaughlin Research Institute Animal Resource Center staff for animal care, and Sarah Anderson for assistance with mouse genotyping. This work was funded by R21 NS070246 from the National Institute of Neurological Disorders and Stroke and generous supporters of the McLaughlin Research Institute. The funders had no role in study design, data collection or analysis, decision to publish, or preparation of the manuscript.

References

Ashrafi G, Schwarz TL, 2013 The pathways of mitophagy for quality control and clearance of mitochondria. Cell Death Differ. 20, 31–42. [PubMed: 22743996]

Benvegnu S, Wahle T, Dotti CG, 2017 E3 ligase mahogunin (MGRN1) influences amyloid precursor protein maturation and secretion. Oncotarget 8, 89439–89450. [PubMed: 29163761]

Betts J, Lightowlers RN, Turnbull DM, 2004 Neuropathological aspects of mitochondrial DNA disease. Neurochem Res 29, 505–511. [PubMed: 15038598]

Brown GK, Squier MV, 1996 Neuropathology and pathogenesis of mitochondrial diseases. J. Inherit. Metab. Dis 19, 553–572. [PubMed: 8884579]

Chen H, Chan DC, 2009 Mitochondrial dynamics--fusion, fission, movement, and mitophagy--in neurodegenerative diseases. Hum. Mol. Genet 18, R169–176. [PubMed: 19808793]

Chen H, Chomyn A, Chan DC, 2005 Disruption of fusion results in mitochondrial heterogeneity and dysfunction. J. Biol. Chem 280, 26185–26192. [PubMed: 15899901]

Choi SI, Ju WK, Choi EK, Kim J, Lea HZ, Carp RI, Wisniewski HM, Kim YS, 1998 Mitochondrial dysfunction induced by oxidative stress in the brains of hamsters infected with the 263 K scrapie agent. Acta Neuropathol 96, 279–286. [PubMed: 9754961]

Cota CD, Bagher P, Pelc P, Smith CO, Bodner CR, Gunn TM, 2006 Mice with mutations in Mahogunin ring finger-1 (Mgrn1) exhibit abnormal patterning of the left-right axis. Dev. Dyn 235, 3438–3447. [PubMed: 17075880]

Dagda RK, Cherra SJ 3rd, Kulich SM, Tandon A, Park D, Chu CT, 2009 Loss of PINK1 Function Promotes Mitophagy through Effects on Oxidative Stress and Mitochondrial Fission. J. Biol. Chem 284, 13843–13855. [PubMed: 19279012]

Damiano M, Gautier CA, Bulteau AL, Ferrando-Miguel R, Gouarne C, Paoli MG, Pruss R, Auchere F, L'Hermitte-Stead C, Bouillaud F, Brice A, Corti O, Lombes A, 2014 Tissue- and cell-specific mitochondrial defect in Parkin-deficient mice. PLoS One 9, e99898. [PubMed: 24959870]

Deng H, Dodson MW, Huang H, Guo M, 2008 The Parkinson's disease genes pink1 and parkin promote mitochondrial fission and/or inhibit fusion in Drosophila. Proc. Natl. Acad. Sci. U. S. A 105, 14503–14508. [PubMed: 18799731]

Exner N, Treske B, Paquet D, Holmstrom K, Schiesling C, Gispert S, Carballo-Carbajal I, Berg D, Hoepken HH, Gasser T, Kruger R, Winklhofer KF, Vogel F, Reichert AS, Auburger G, Kahle PJ, Schmid B, Haass C, 2007 Loss-of-function of human PINK1 results in mitochondrial pathology and can be rescued by parkin. J. Neurosci 27, 12413–12418. [PubMed: 17989306]

Filosto M, Tomelleri G, Tonin P, Scarpelli M, Vattemi G, Rizzuto N, Padovani A, Simonati A, 2007 Neuropathology of mitochondrial diseases. Biosci. Rep 27, 23–30. [PubMed: 17541738]

Finsterer J, 2006 Central nervous system manifestations of mitochondrial disorders. Acta Neurol. Scand 114, 217–238. [PubMed: 16942541]

Gautier CA, Kitada T, Shen J, 2008 Loss of PINK1 causes mitochondrial functional defects and increased sensitivity to oxidative stress. Proc. Natl. Acad. Sci. U. S. A 105, 11364–11369. [PubMed: 18687901]

He L, Lu XY, Jolly AF, Eldridge AG, Watson SJ, Jackson PK, Barsh GS, Gunn TM, 2003 Spongiform degeneration in mahoganoid mutant mice. Science 299, 710–712. [PubMed: 12560552]

Hida T, Wakamatsu K, Sviderskaya EV, Donkin AJ, Montoliu L, Lynn Lamoreux M, Yu B, Millhauser GL, Ito S, Barsh GS, Jimbow K, Bennett DC, 2009 Agouti protein, mahogunin, and attractin in pheomelanogenesis and melanoblast-like alteration of melanocytes: a cAMP-independent pathway. Pigment Cell Melanoma Res 22, 623–634. [PubMed: 19493315]

Jiao J, Kim HY, Liu RR, Hogan CA, Sun K, Tam LM, Gunn TM, 2009a Transgenic analysis of the physiological functions of Mahogunin Ring Finger-1 isoforms. Genesis 47, 524–534. [PubMed: 19422019]

Jiao J, Sun K, Walker WP, Bagher P, Cota CD, Gunn TM, 2009b Abnormal regulation of TSG101 in mice with spongiform neurodegeneration. Biochim. Biophys. Acta 1792, 1027–1035. [PubMed: 19703557]

Kim BY, Olzmann JA, Barsh GS, Chin LS, Li L, 2007 Spongiform neurodegeneration-associated E3 ligase Mahogunin ubiquitylates TSG101 and regulates endosomal trafficking. Mol. Biol. Cell 18, 1129–1142. [PubMed: 17229889]

Leone TC, Lehman JJ, Finck BN, Schaeffer PJ, Wende AR, Boudina S, Courtois M, Wozniak DF, Sambandam N, Bernal-Mizrachi C, Chen Z, Holloszy JO, Medeiros DM, Schmidt RE, Saffitz JE, Abel ED, Semenkovich CF, Kelly DP, 2005 PGC-1alpha deficiency causes multi-system energy metabolic derangements: muscle dysfunction, abnormal weight control and hepatic steatosis. PLoS Biol 3, e101. [PubMed: 15760270]

Livak KJ, Schmittgen TD, 2001 Analysis of relative gene expression data using real-time quantitative PCR and the 2(-Delta Delta C(T)) Method. Methods 25, 402–408. [PubMed: 11846609]

Matsuda N, Sato S, Shiba K, Okatsu K, Saisho K, Gautier CA, Sou YS, Saiki S, Kawajiri S, Sato F, Kimura M, Komatsu M, Hattori N, Tanaka K, 2010 PINK1 stabilized by mitochondrial depolarization recruits Parkin to damaged mitochondria and activates latent Parkin for mitophagy. J. Cell Biol 189, 211–221. [PubMed: 20404107]

Meyer JN, Leuthner TC, Luz AL, 2017 Mitochondrial fusion, fission, and mitochondrial toxicity. Toxicology.

Mukherjee R, Chakrabarti O, 2016a Regulation of Mitofusin1 by Mahogunin Ring Finger-1 and the proteasome modulates mitochondrial fusion. Biochim. Biophys. Acta 1863, 3065–3083. [PubMed: 27713096]

Mukherjee R, Chakrabarti O, 2016b Ubiquitin-mediated regulation of the E3 ligase GP78 by MGRN1 in trans affects mitochondrial homeostasis. J. Cell Sci. 129, 757–773. [PubMed: 26743086]

Narendra D, Tanaka A, Suen DF, Youle RJ, 2008 Parkin is recruited selectively to impaired mitochondria and promotes their autophagy. J. Cell Biol. 183, 795–803. [PubMed: 19029340]

Narendra D, Tanaka A, Suen DF, Youle RJ, 2009 Parkin-induced mitophagy in the pathogenesis of Parkinson disease. Autophagy 5.

Palacino JJ, Sagi D, Goldberg MS, Krauss S, Motz C, Wacker M, Klose J, Shen J, 2004 Mitochondrial dysfunction and oxidative damage in parkin-deficient mice. J. Biol. Chem 279, 18614–18622. [PubMed: 14985362]

Pan Y, Chen H, Siu F, Kilberg MS, 2003 Amino acid deprivation and endoplasmic reticulum stress induce expression of multiple activating transcription factor-3 mRNA species that, when overexpressed in HepG2 cells, modulate transcription by the human asparagine synthetase promoter. J. Biol. Chem 278, 38402–38412. [PubMed: 12881527]

Pan YX, Chen H, Thiaville MM, Kilberg MS, 2007 Activation of the ATF3 gene through a co-ordinated amino acid-sensing response programme that controls transcriptional regulation of responsive genes following amino acid limitation. Biochem. J 401, 299–307. [PubMed: 16989641]

Poole AC, Thomas RE, Andrews LA, McBride HM, Whitworth AJ, Pallanck LJ, 2008 The PINK1/Parkin pathway regulates mitochondrial morphology. Proc. Natl. Acad. Sci. U. S. A 105, 1638–1643. [PubMed: 18230723]

Pusapati GV, Kong JH, Patel BB, Krishnan A, Sagner A, Kinnebrew M, Briscoe J, Aravind L, Rohatgi R, 2018 CRISPR Screens Uncover Genes that Regulate Target Cell Sensitivity to the Morphogen Sonic Hedgehog. Dev Cell 44, 271. [PubMed: 29401421]

Quintana A, Kruse SE, Kapur RP, Sanz E, Palmiter RD, 2010 Complex I deficiency due to loss of Ndufs4 in the brain results in progressive encephalopathy resembling Leigh syndrome. Proc. Natl. Acad. Sci. U. S. A 107, 10996–11001. [PubMed: 20534480]

Quiros PM, Prado MA, Zamboni N, D'Amico D, Williams RW, Finley D, Gygi SP, Auwerx J, 2017 Multi-omics analysis identifies ATF4 as a key regulator of the mitochondrial stress response in mammals. J. Cell Biol. 216, 2027–2045. [PubMed: 28566324]

Ruhoy IS, Saneto RP, 2014 The genetics of Leigh syndrome and its implications for clinical practice and risk management. The application of clinical genetics 7, 221–234. [PubMed: 25419155]

Shah A, Kumar A, 2016 HIV-1 gp120-Mediated Mitochondrial Dysfunction and HIV-Associated Neurological Disorders. Neurotox Res 30, 135–137. [PubMed: 27072361]

Silvius D, Pitstick R, Ahn M, Meishery D, Oehler A, Barsh GS, DeArmond SJ, Carlson GA, Gunn TM, 2013 Levels of the Mahogunin Ring Finger 1 E3 ubiquitin ligase do not influence prion disease. PLoS One 8, e55575. [PubMed: 23383230]

Siskova Z, Mahad DJ, Pudney C, Campbell G, Cadogan M, Asuni A, O'Connor V, Perry VH, 2010 Morphological and functional abnormalities in mitochondria associated with synaptic degeneration in prion disease. Am. J. Pathol 177, 1411–1421. [PubMed: 20651247]

Sterky FH, Lee S, Wibom R, Olson L, Larsson NG, 2011 Impaired mitochondrial transport and Parkin-independent degeneration of respiratory chain-deficient dopamine neurons in vivo. Proc. Natl. Acad. Sci. U. S. A 108, 12937–12942. [PubMed: 21768369]

Sun K, Johnson BS, Gunn TM, 2007 Mitochondrial dysfunction precedes neurodegeneration in Mahogunin (Mgrn1) mutant mice. Neurobiol. Aging 28, 1840–1852. [PubMed: 17720281]

Szalardy L, Zadori D, Plangar I, Vecsei L, Weydt P, Ludolph AC, Klivenyi P, Kovacs GG, 2013 Neuropathology of partial PGC-1alpha deficiency recapitulates features of mitochondrial encephalopathies but not of neurodegenerative diseases. Neurodegener Dis 12, 177–188. [PubMed: 23406886]

Tanji K, Kunimatsu T, Vu TH, Bonilla E, 2001 Neuropathological features of mitochondrial disorders. Semin Cell Dev Biol 12, 429–439. [PubMed: 11735377]

Villa E, Marchetti S, Ricci JE, 2018 No Parkin Zone: Mitophagy without Parkin. Trends Cell Biol. 28, 882–895. [PubMed: 30115557]

Walker WP, Oehler A, Edinger AL, Wagner KU, Gunn TM, 2016 Oligodendroglial deletion of ESCRT-I component TSG101 causes spongiform encephalopathy. Biol. Cell 108, 324–337. [PubMed: 27406702]

Wells GA, Wells M, 1989 Neuropil vacuolation in brain: a reproducible histological processing artefact. J. Comp. Pathol 101, 355–362. [PubMed: 2691536]

Yang W, Wang G, Wang CE, Guo X, Yin P, Gao J, Tu Z, Wang Z, Wu J, Hu X, Li S, Li XJ, 2015 Mutant alpha-synuclein causes age-dependent neuropathology in monkey brain. J. Neurosci 35, 8345–8358. [PubMed: 26019347]

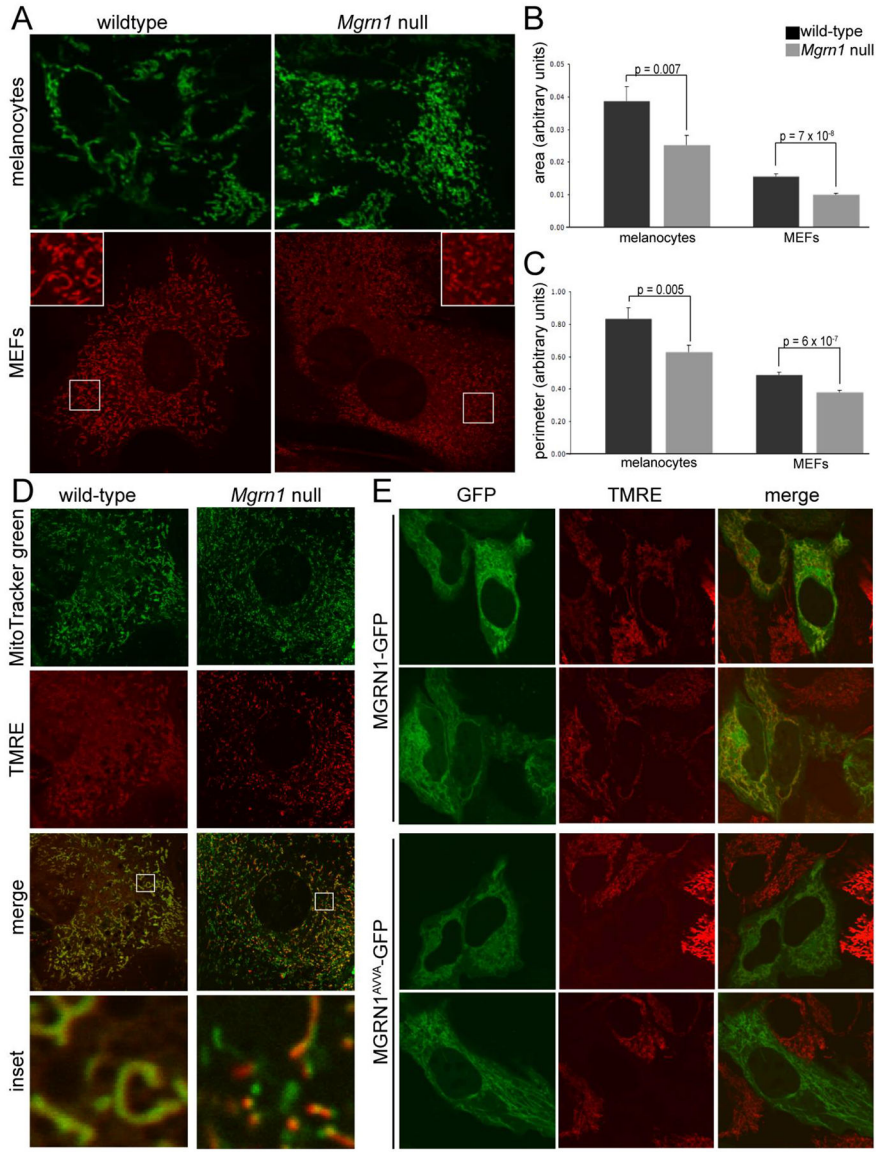

Fig. 1. Disruption of MGRN1 affects mitochondrial morphology and membrane potential.

(A-C) Representative confocal images of live wildtype and *Mgrn1* null melanocytes (upper panels) and MEFs (lower panels) stained with MitoTracker green or MitoTracker red (A). Mitochondrial area (B) and perimeter (C) were measured on >20 cells per cell type and genotype in each of 5 independent cultures using ImageJ, and statistical analysis performed using Student's *t*-test. (D) Representative confocal images of live wildtype and *Mgrn1* null MEFs stained with MitoTracker green, then with TMRE, showing punctate TMRE staining in *Mgrn1* null cells. (E) Representative confocal images of live HeLa cells transfected with MGRN1-GFP or MGRN1^{AVVA}-GFP and stained with TMRE. Diminished TMRE staining in cells expressing MGRN1^{AVVA}-GFP suggests that this catalytically inactive mutant has dominant negative activity that disrupts mitochondrial membrane polarization.

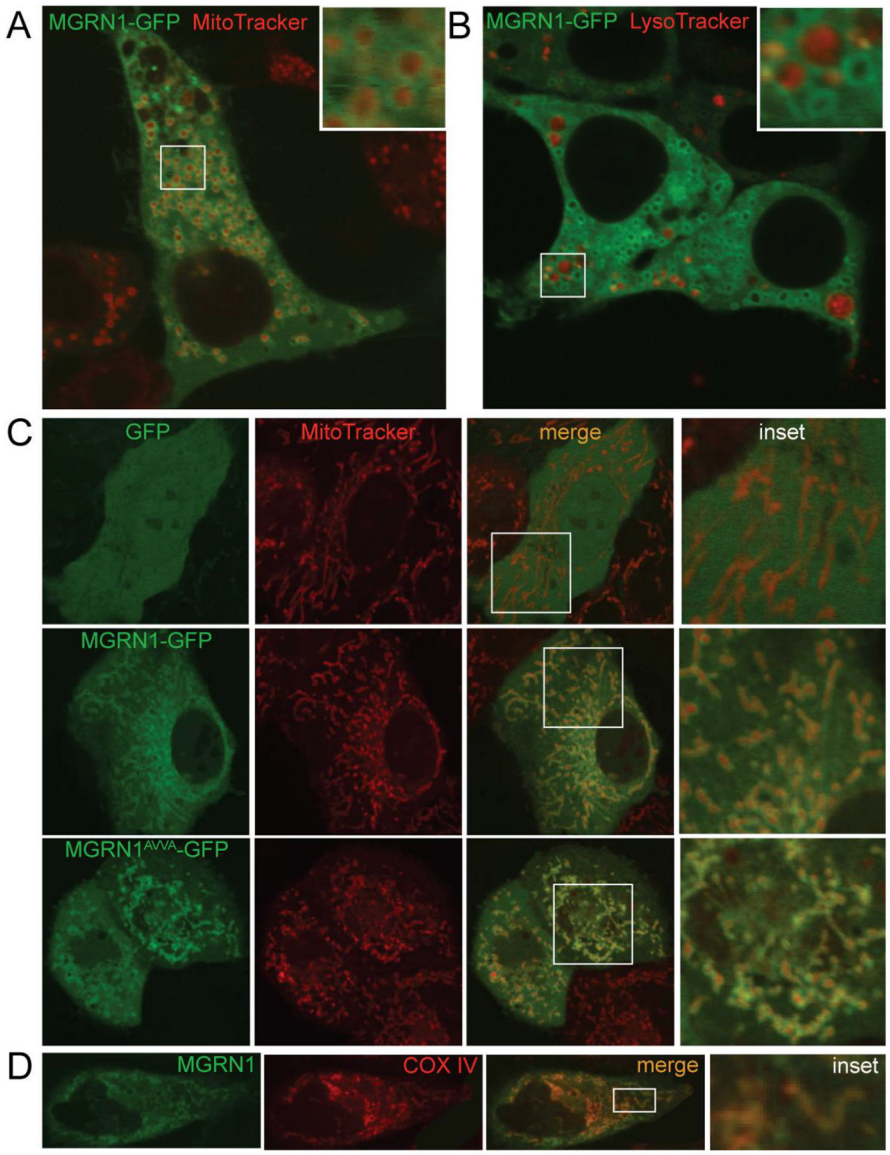

Fig. 2. Mitochondrial localization of MGRN1.

(A-B) Confocal images of HEK293T cells transfected with MGRN1-GFP and stained with MitoTracker Red (A) or LysoTracker Red (B). MGRN1-GFP surrounded virtually all MitoTracker-stained structures but colocalized with only a subset of LysoTracker-stained lysosomes. (C) Confocal images of HeLa cells transfected with GFP, MGRN1-GFP or MGRN1^{AVVA}-GFP and stained with MitoTracker red. While GFP was diffusely cytoplasmic, MGRN1-GFP and MGRN1^{AVVA}-GFP showed cytoplasmic staining as well as mitochondrial localization that appeared to encircle MitoTracker red stained structures. (D) Confocal images of HeLa cells following immunocytochemistry for the inner mitochondrial membrane protein cytochrome c oxidase, subunit IV (COX IV, red) and MGRN1 (green) demonstrate both mitochondrial and cytoplasmic localization of endogenous MGRN1. (E-F) Confocal images of HeLa cells transfected with wildtype MGRN1-HIS (E) or MGRN1^{G2A}-HIS (F) following immunocytochemistry for COX IV (green) and the HIS tag (red).

Wildtype MGRN1-HIS colocalized with COX IV (indicated by yellow in merged image) but $MGRN1^{G2A}$-HIS did not.

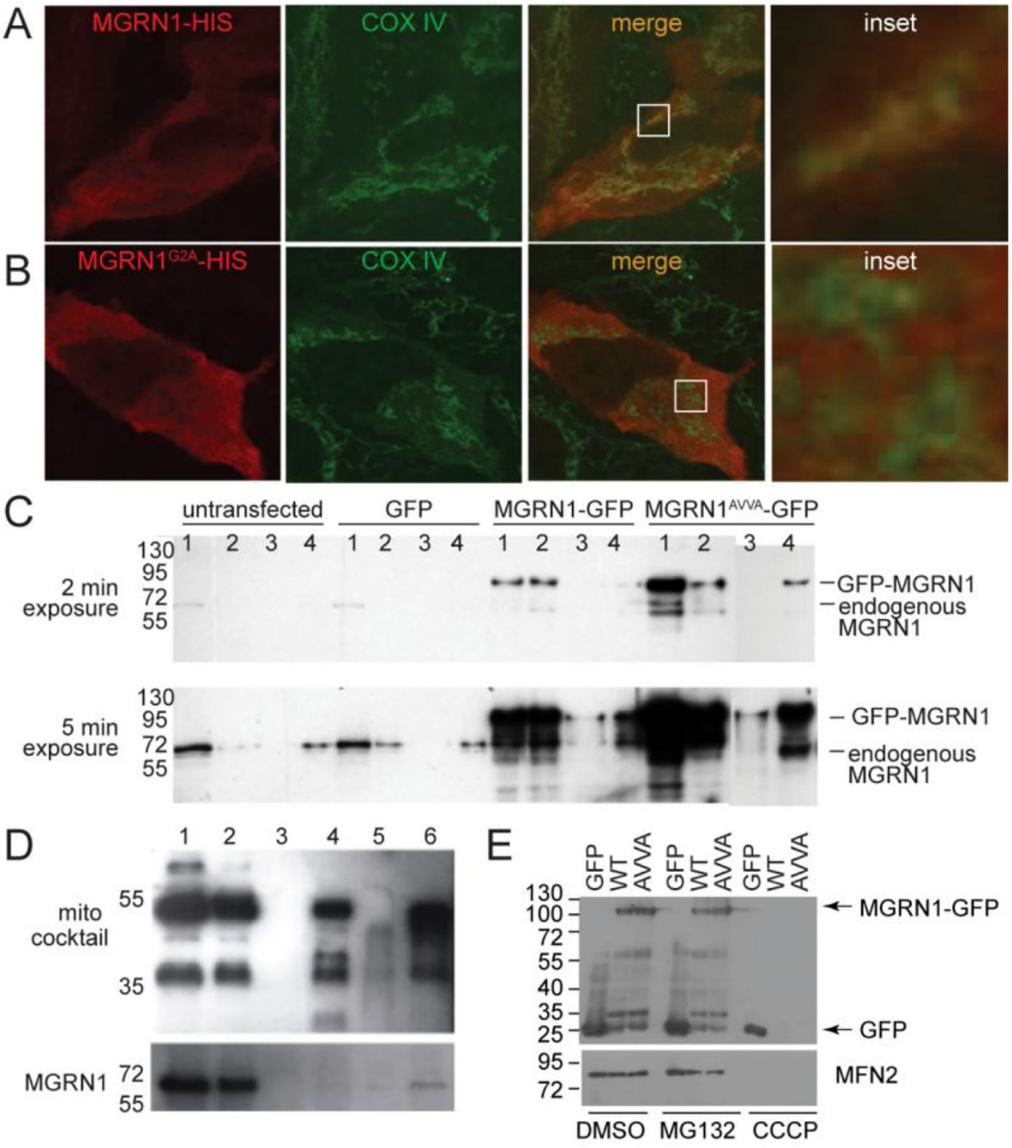

Fig. 3. MGRN1 is tightly associated with mitochondria.

(A-B) Confocal images of HeLa cells transfected with wildtype MGRN1-HIS (A) or MGRN1^{G2A}-HIS (B) following immunocytochemistry for COX IV (green) and the HIS tag (red). (C) Immunoblotting for MGRN1 on whole cell lysates (1), mitochondrial fractions (2), peripheral mitochondrial proteins (Na_2CO_3 supernatent; 3), and integral mitochondrial proteins (Na_2CO_3 pellet; 4) from untransfected HEK293T cells and cells transfected with GFP, MGRN1-GFP or MGRN1^{AVVA}-GFP. Endogenous and wildtype and mutant GFP-tagged MGRN1 were detected in whole cell lysates, mitochondrial fractions and the Na_2CO_3 pellet. (D) HEK293T whole cell lysate (1), mitochondria fraction (2), the supernatent (3) or pellet (4) following trypsin digestion of the mitochondrial fraction, and the supernatent (5) or pellet (6) from proteinase K digestion of the mitochondrial fraction were immunoblotted with an antibody cocktail against several mitochondrial proteins (top panel) or an antibody against MGRN1. (E) HEK293T cells transfected with GFP, MGRN1-

GFP or MGRN1^{AVVA}-GFP were treated overnight with DMSO (vehicle control), MG132 or CCCP, and whole cell lysates were immunoblotted for GFP (upper panel) and the outer mitochondrial membrane protein mitofusin-2 (MFN2) (lower panel).

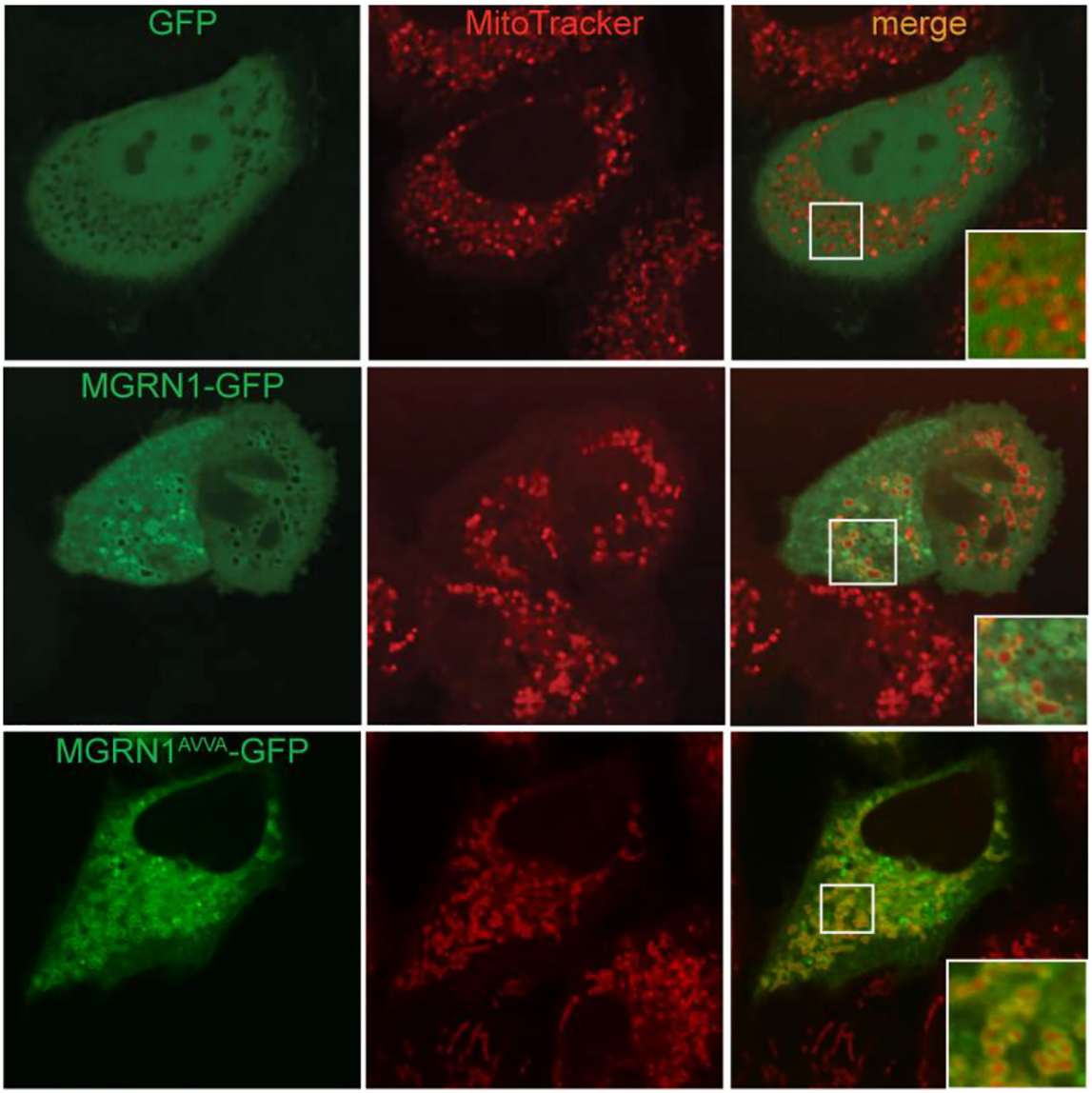

Fig. 4. MGRN1 remains localized to mitochondrial following CCCP treatment.

Confocal images of HeLa cells transfected with GFP, MGRN1-GFP or MGRN1^{AVVA}-GFP that were preloaded with MitoTracker red, then treated with 10 μM CCCP for 2 hours. CCCP treatment did not affect localization of wildtype or AVVA mutant MGRN1-GFP to mitochondria.

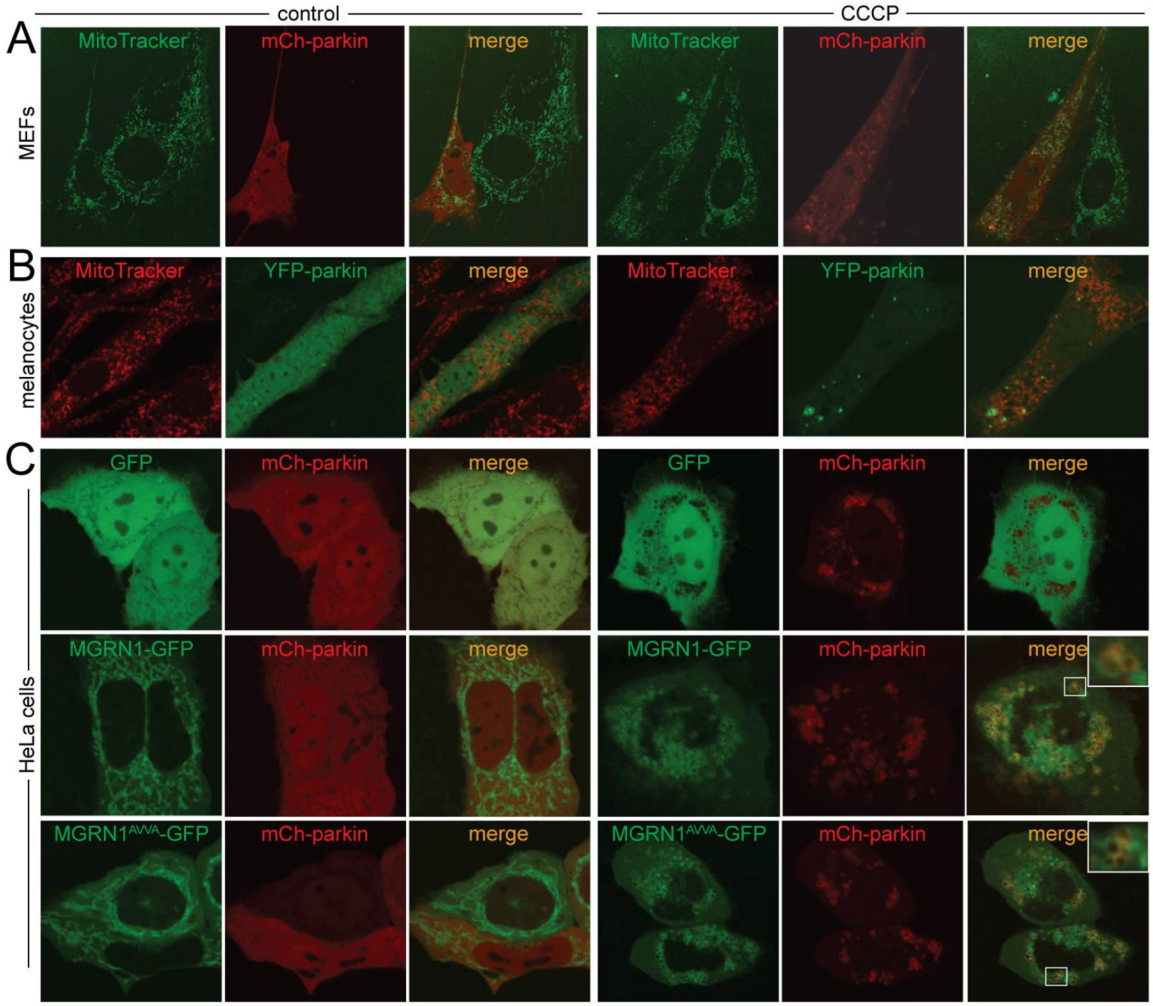

Fig. 5. MGRN1 does not affect parkin recruitment.

(A) Representative confocal images of *Mgrn1* null MEFs transfected with mCh-parkin, stained with MitoTracker green, and imaged before (control) and after 1.5 h CCCP treatment. (B) Representative confocal images of *Mgrn1* null melanocytes transfected with YFP-parkin, stained with MitoTracker red, and imaged after 1.5 h DMSO (control) or CCCP treatment. (C) Representative confocal images of HeLa cells co-transfected with mCh-parkin and GFP, MGRN1-GFP or MGRN1^{AVVA}-GFP that were preloaded with MitoTracker green and imaged before (control) and 2 h after CCCP treatment.

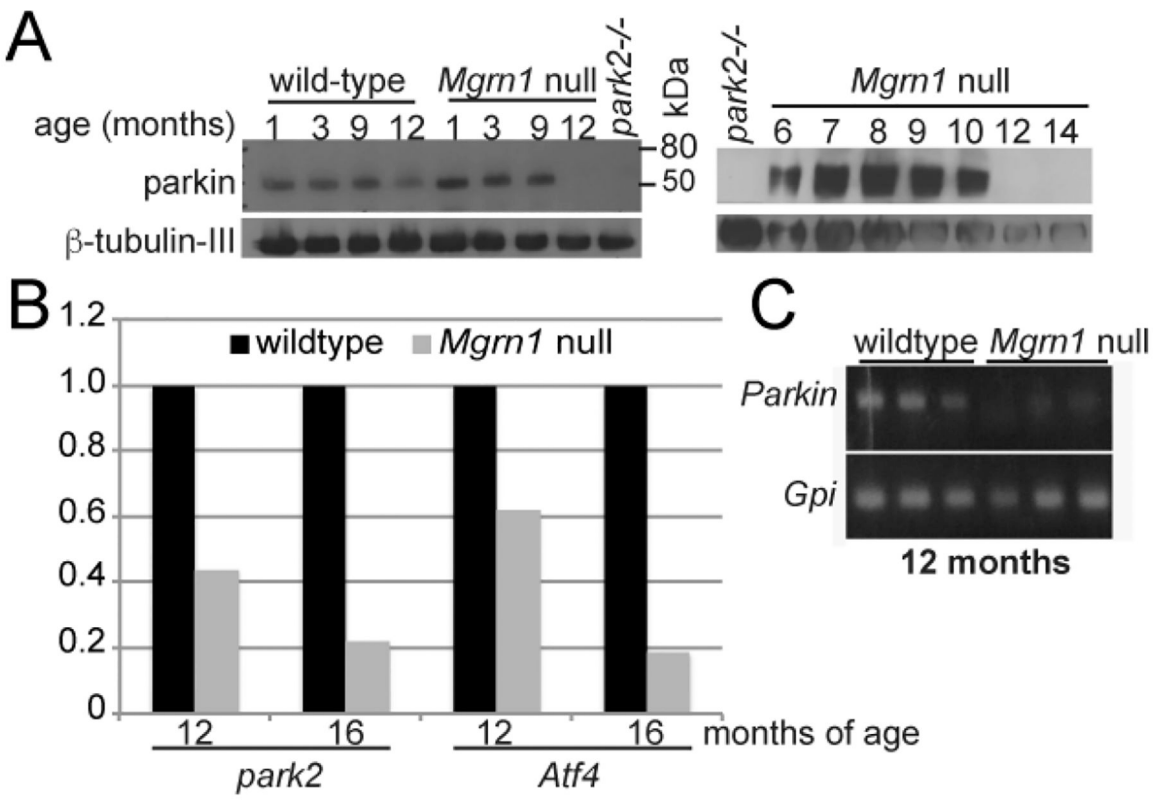

Fig. 6. *Parkin* expression in *Mgrn1* null brains.

(A) Whole brain lysates from wildtype, *Mgrn1* null and *parkin* null mutant mice at the indicated ages immunoblotted for parkin. *Mgrn1* mutant samples consistently showed little or no parkin expression by 12 months of age. β-tubulin-III on the same blots shows equivalent protein loading. (B) Quantitative RT-PCR demonstrates reduced *parkin* and *Atf4* expression in the brains of aged *Mgrn1* null mutant mice. (C) Agarose gel of RT-PCR products from 12-month-old animals, showing significant reduction of *parkin* in *Mgrn1* null mutant brains.

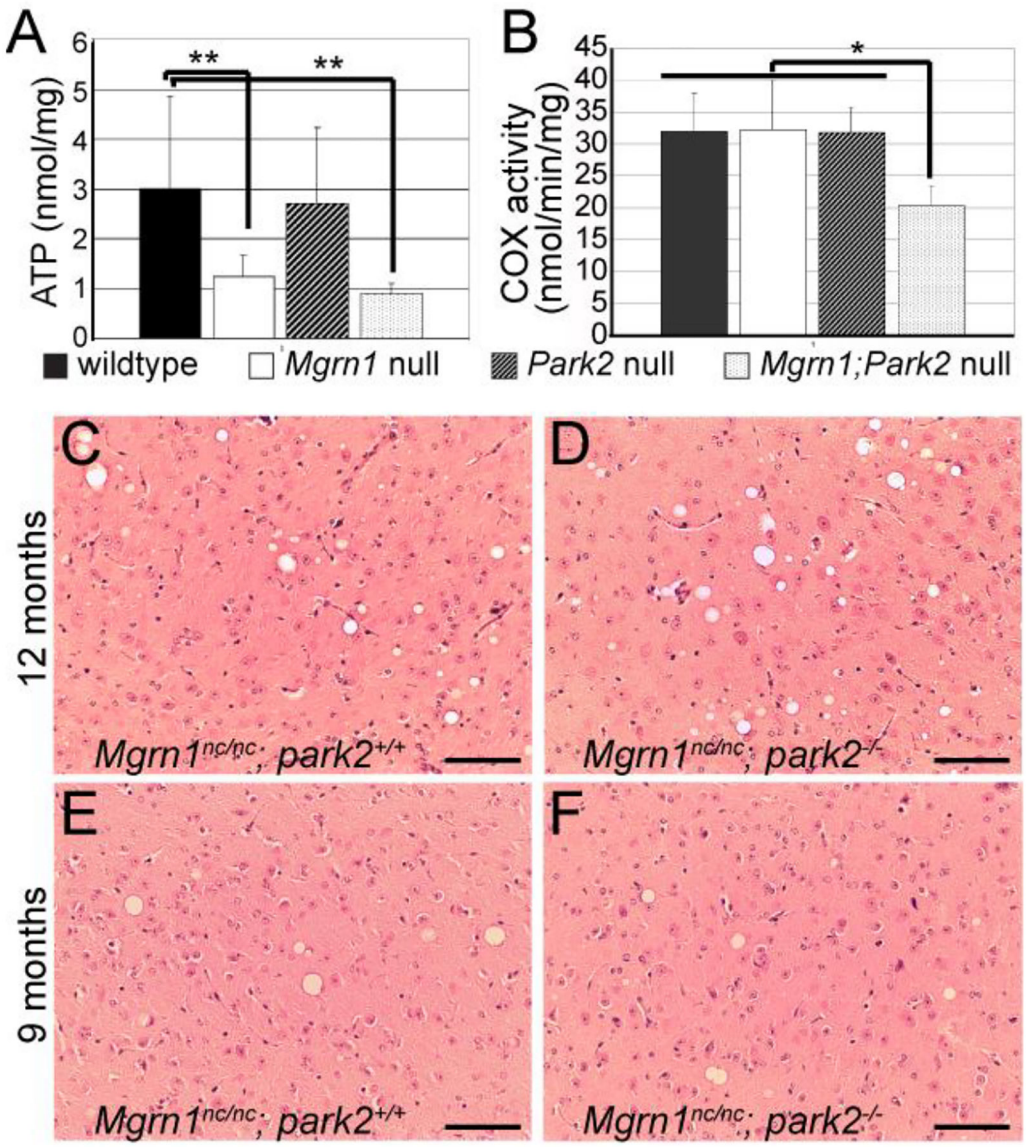

Fig. 7. Synergistic effects of MGRN1 and parkin.

(A-B) ATP levels (A) and cytochrome c oxidase (COX) activity (B) in whole brain lysates of 1-month old wildtype, *Mgrn1* null, *park2* null and *Mgrn1; park2* double mutant mice. **p<0.04; *p<0.007. The difference in ATP levels between *Mgrn1* null and double mutant brains was suggestive but not significant (p=0.098). (C-F) Representative hematoxylin and eosin stained 5 μm sagittal sections of the thalamus of 9-(C, D) and 12-(E, F) month-old $Mgrn1^{md\text{-}nc/md\text{-}nc}$; $park2^{+/+}$ (C, E) and $Mgrn1^{md\text{-}nc/md\text{-}nc}$; $park2^{-/-}$ (D, F) mice. Scale bars: 10 μm.

Table 1.

Relative expression of *parkin* and *Atf4* in the brains of aged wildtype and *Mgrn1* null mutant mice

Gene	Age (months)	Relative expression[a] (range)		
		Wildtype	*Mgrn1*$^{md\text{-}nc/md\text{-}nc}$	*t*-test p value[b]
Parkin	12	1 [0.76–1.32]	0.44 [0.36–0.54]	0.015*
	16	1 [0.68–1.48]	0.22 [0.11–0.47]	0.037*
Atf4	12	1 [0.68–1.47]	0.62 [0.42–0.93]	0.211
	16	1 [0.76–1.32]	0.19 [0.14–0.26]	0.002*

[a] ΔΔCT method, normalized against *Gpi*, with wildtype set to 1.0

[b] Statistically significant differences denoted by *

Table 2.

Effect of *parkin* deletion on severity of CNS vacuolation[†] in *Mgrn1* null mutant mice

		Cerebellum					
Age (months)	**Genotype**	**White matter**	**Granule layer**	**Molecular layer**	**Pons**	**Thalamus**	**Hippocampus**
12	*Mgrn1*$^{md\text{-}nc/md\text{-}nc}$; parkin$^{+/+}$	1	1	0	1	3	2
12	*Mgrn1*$^{md\text{-}nc/md\text{-}nc}$; parkin$^{-/-}$	1	1	0	1	4	2
9	*Mgrn1*$^{md\text{-}nc/md\text{-}nc}$; parkin$^{+/+}$	0	0	0	1	2	1
9	*Mgrn1*$^{md\text{-}nc/md\text{-}nc}$; parkin$^{-/-}$	0	0	0	1	2	1

[†]Scoring was based on average number of vacuoles in the field of view at 20X magnification as follows: 0 = no significant lesions (0–1 vacuoles); 1 = rare, scattered vacuoles (2–5 vacuoles, not present in all fields of view); 2 = mild, 6–10 scattered vacuoles in all fields of view; 3 = moderate, vacuoles in every field of view and 11–29 evenly scattered vacuoles in most; 4 = severe, > 30 vacuoles in all fields of view.